Atmos. Meas. Tech. Discuss., https://doi.org/10.5194/amt-2018-177
Manuscript under review for journal Atmos. Meas. Tech.
Discussion started: 13 June 2018

Atmospheric Measurement Techniques Discussions

An instrument for quantifying heterogeneous ice nucleation in multiwell plates using infrared emissions to detect freezing

Alexander D. Harrison[1], Thomas F. Whale[1], Rupert Rutledge[2], Stephen Lamb[2], Mark D. Tarn[1], Grace C. E. Porter[1], Michael Adams[1], James B. McQuaid[1], George J. Morris[2] and Benjamin J. Murray[1]

[1]School of Earth and Environment, University of Leeds, Leeds, LS2 9JT

[2]Asymptote Ltd., GE Healthcare, Sovereign House, Cambridge, CB24 9BZ

Correspondence to: A. D. Harrison (ee11ah@leeds.ac.uk) and B. J. Murray (b.j.murray@leeds.ac.uk)

Abstract

Low concentrations of ice nucleating particles (INPs) are thought to be important for the properties of mixed-phase clouds, but their detection is challenging. While instruments to quantify INPs online can provide relatively high time resolution data, they typically cannot quantify very low INP concentrations. Furthermore, typical online instruments tend to report data at a single defined set of conditions. Hence, there is a need for instruments where INP concentrations of less than 0.01 L^{-1} can be routinely and efficiently determined. The use of larger volumes of suspension in drop assays increases the sensitivity of an experiment to rarer INPs or rarer active sites due to the increase in aerosol or surface area of particulates per droplet**.** Here we describe and characterise the InfraRed-Nucleation by Immersed Particles Instrument (IR-NIPI), a new immersion freezing assay that makes use of IR emissions to determine the freezing temperature of individual 50µL droplets each contained in a well of a 96-well plate. Using an IR camera allows the temperature of individual aliquots to be monitored. Freezing temperatures are determined by detecting the sharp rise in well temperature associated with the release of heat caused by freezing. In this paper we first present the calibration of the IR temperature measurement, which makes use of the freezing period after initial nucleation when wells warm and their temperature is determined by the ice-liquid equilibrium temperature, i.e. 0°C when the water activity is ~1. We then tested the temperature calibration using ~100 µm chips of K-feldspar, by immersing these chips in 1 µL droplets on an established cold stage (µL-NIPI) as well as in 50 µL droplets on IR-NIPI; the results were consistent with one another indicating no bias in the reported freezing temperature. In addition we present measurements of the efficiency of the mineral dust NX-illite and a sample of atmospheric aerosol collected on a filter in the city of Leeds. NX-illite results are consistent with

literature data and the atmospheric INP concentrations were in good agreement with the results from the µL-NIPI instrument. This demonstrates the utility of this approach, which offers a relatively high throughput of sample analysis and access to low INP concentrations.

1 Introduction

Cloud droplets can freeze homogeneously below about -33°C (Herbert et al., 2015), but the presence of ice-nucleating particles (INPs) can induce freezing at much warmer temperatures (Kanji et al., 2017). The glaciation of clouds at these warmer temperatures has a substantial impact on a cloud's reflective properties, lifetime and therefore the overall climate of the planet, but is poorly represented in many models (Hoose and Möhler, 2012; Vergara-Temprado et al., 2018). INPs can cause nucleation through a number of pathways (Vali et al., 2015), but in mixed-phase clouds it is thought that the pathways where particles become immersed in droplets is most important (Hoose et al., 2010; Murray et al., 2012). Even small concentrations of INPs can influence cloud properties; for example, in a modelling study of Southern Ocean shallow mixed-phase clouds, Vergara-Temprado et al. (2018) showed that while concentrations of INPs greater than ~1 L^{-1} cause profound changes in cloud properties, clouds are sensitive to concentrations many orders of magnitude smaller.

The ability to quantify INP spectra (INP concentrations as a function of temperature) and test the efficiency of proxy materials for ice-nucleating efficiency is invaluable for improving our understanding of cloud glaciation. However it is not a trivial task, in part because INP concentrations are low and the sites on surfaces which cause nucleation at warm temperatures are rare. There are several different methods of conducting ice nucleation experiments that include Continuous Flow Diffusion Chambers (CFDC's) e.g. (Salam et al., 2006; Rogers et al., 2001), cloud expansion chambers e.g. (Niemand et al., 2012; Cotton et al., 2007), wind tunnels e.g. (Pitter and Pruppacher, 1973; Diehl and Mitra, 1998) and droplet freezing assays e.g. (Knopf and Alpert, 2013; Vali, 2008; Murray et al., 2011; Budke and Koop, 2015; Whale et al., 2015; Beall et al., 2017). Each of these systems has its limitations and advantages which must be understood and accounted for when conducting an experiment and interpreting the results. For example CFDCs cannot be used for measurements at temperatures warmer than about -11°C but they do allow for specific saturation conditions to be controlled, something which other instruments cannot achieve. For more information on the capabilities and limitations of the various techniques see the comprehensive review and intercomparison which was conducted by Hiranuma *et al.* (2015).

A significant challenge in sampling INPs in the atmosphere is their low concentration. At present there is a dearth of published, atmospherically relevant, INP measurements globally (Vergara-Temprado et al., 2017). Not only is

the global spatial and temporal coverage of INPs inadequate, but the range of activation temperatures and INP concentrations covered in any one set of measurements is typically limited. No single instrument has the capability of measuring INP concentrations over the full range of conditions relevant to mixed-phase clouds. Online instruments, such as CFDCs, do precisely this, but their detection limit is limited to ~10^{-1} L^{-1} (Eidhammer et al., 2010). This can be improved with aerosol concentrators, but is still above the INP concentrations models suggest influence the properties of certain cloud types, such as shallow cold-sector clouds in the Southern Ocean (Vergara-Temprado et al., 2018). The alternative approach is therefore to increase the number of particles within each aliquot of water. In principle, if the ice-nucleating properties of the aerosol particles in question are insensitive to mixing state, then increasing the amount of aerosol per droplet will scale with inverse proportionality to the INP concentration, thereby allowing quantification of lower INP concentrations. To increase the number of aerosol particles per volume of liquid the time period over which an atmospheric sample is collected can be extended, but in doing so temporal resolution would be lost. An alternative method of increasing the sensitivity of an immersion mode technique is to increase the volume of suspension used in each aliquot. This has been done in the past e.g. (Vali, 1971; Bigg, 1953), and has been the strategy employed in the development of some recent instruments e.g. (Beall et al., 2017; Du et al., 2017).

Here we propose a new technique, the IR Nucleation by Immersed Particle Instrument (IR-NIPI), for the detection of INPs using large volumes of sample in the immersion mode. This instrument is part of the NIPI suite of instruments that includes the µL-NIPI and when used together these devices allow measurements to be taken over a very wide range of INP concentrations. The use of an infrared camera allows temperature measurements to be made for individual droplets which helps reduce errors from horizontal gradients across the array of droplets and the effect of heat release on the temperature of neighbouring wells. The unique design, in combination with a Stirling engine chiller, is also compact making it ideal for field-based measurements and the use of multiwell plates lends itself to future automation.

2 Instrument Design

2.1 Operating principle

Drop assays have been used extensively for ice nucleation experiments e.g.(Vali, 1971; Vali, 1995; Conen et al., 2011; Knopf and Forrester, 2011; Garcia et al., 2012; Stopelli et al., 2014; Whale et al., 2015; Budke and Koop, 2015). This is partly due to their simplicity compared to other techniques but also the ability to scale the amount of nucleator with droplet size. In brief, aqueous suspensions are prepared and droplets of a well quantified size

are placed onto a substrate or immersed in oil. These droplets tend to be monodispersed but polydispersed experiments are also possible (Vali, 1971; Murray et al., 2011). The system is then cooled and the fraction of droplets frozen is recorded. The cooling can be conducted at a constant rate or with a stepped rate to hold the droplets at a specified temperature for a period of time (i.e. isothermally) to explore the time dependence aspect of ice nucleation (Herbert et al., 2014; Vali, 1994; Sear, 2014). The droplets are monitored and the freezing temperature of each droplet is recorded. The fraction of the droplet population frozen throughout the explored temperature range can then be determined, from which other expressions of the ice-nucleating properties or INP concentrations can be derived (Vali et al., 2015).

If the surface area of nucleant per droplet is known then it is common to express the nucleating ability of a material as the density of active sites per unit surface area of nucleator, $n_s(T)$ (Connolly et al., 2009; DeMott, 1995). This approach is based on the assumption specific sites on a nucleator's surface are responsible for ice formation. n_s is a cumulative term, i.e. as you move to cooler temperatures there are more features which may behave as an active site as the energy barrier for ice formation decreases. $n_s(T)$ is calculated via equation (1).

$$n_{S=} \frac{(-\ln(1-\frac{n(T)}{N}))}{A} \quad (1)$$

Where $n(T)$ is the number of droplets frozen at a given temperature and N is the total number of droplets. A is the surface area of nucleator within each droplet. Nucleation is a time-dependent stochastic process, but in determining $n_s(T)$ the time dependence is neglected. This assumption is justified for many materials because the diversity in activity of active sites leads to a much greater spread in freezing temperatures than the shift in freezing temperatures associated with changes in cooling rate (Vali, 2008; Herbert et al., 2014).

2.2 IR-NIPI design

In brief an aqueous suspension is prepared and aliquots pipetted into the wells of a 96 multiwell plate which is then placed on a temperature controlled stage. The cold stage and multiwell plate are enclosed by a Perspex cover with an infrared camera mounted in its lid (Figure 1). The system is cooled at ~ -1°C min^{-1} until all droplets are frozen (typically in a temperature range of 0 to -30°C). The temperature of the individual aliquots is monitored using the IR camera which records a temperature map every 20 seconds. The temperature map is then analysed with a semi-automated process using custom Python code to yield the freezing temperatures of individual wells.

The IR-NIPI has been designed around an Asymptote Ltd. VIA Freeze™ stirling cryocooler (Figure 1). The VIA Freeze uses a Stirling engine to provide a convenient means of cooling without refrigerants or circulating liquids and was primarily designed for use in cryopreservation applications. This chiller can achieve temperatures of -90°C, hence it has more than enough cooling capacity for our application, and has sufficiently low power requirements that allow it to be run from an automotive 12 V inverter. It also features an onboard datalogger and internal computer with touch screen control. The VIA Freeze has been developed to accommodate multiwell plates onto its aluminium cooling stage, which are ideal for large volume drop assays as they hold up to 200 µL per aliquot (for the 96 well plates), allow the separation of droplets to reduce interference across cells and can be supplied medically sterile. These multiwell plates have anywhere from 12-1536 (with maximum working volumes of 6.9 mL to 2 µL, respectively). The most useful for this freezing assay are the 96 x 200 µL or 384 x 50 µL aliquot arrays and in the tests reported here 50µL droplets are used in 96 well plates. We have used both polystyrene (Corning, CLS3788) and polypropylene plates (Greiner, M8060) and observed no difference in freezing results between the two. To aid thermal contact between the multiwell plate and the VIA Freeze a thermally conductive gap pad (RS components, 7073452) is located between the cold plate and the multiwell plate, while a clamping system with screw threads applies mechanical pressure to the multiwell plate to push the wells into the pad (Figure 1). A specially designed Perspex hood then encloses the system to reduce contamination from the surroundings. The IR camera slots into the hood and captures an image of the multiwell plate every 20 seconds (Figure 2a), storing the corresponding temperature data (Figure 2b) on a removable memory card. The IR camera used here is a Fluke Ti9 Thermal Imager with 160 x 120 pixels. The Stirling engine is then set to cool down at 1.3°C min^{-1} which corresponds to 1°C min^{-1} ± 0.06°C in the wells due to a measured offset between the plate and aliquot temperatures. This ramp rate was selected based on preliminary runs and justification for this cooling rate being equivalent to 1°C min^{-1} can be seen in the well temperatures over time (Figure 2b). Once the system has initially cooled to 5°C the temperature is held for 5 min to allow time for the system to equilibrate. Following this the system continues to ramp down in temperature while recording IR heat maps of the multiwell plate.

In order to determine the temperature of individual wells, the analysis code locates a pixel centred in the middle of each well, reporting this temperature as the well temperature. Profiles of temperature versus time are shown in Figure 2b/c. The freezing temperature of each individual well is determined by comparing each temperature reading, for a certain well, with the temperature recorded 20 seconds prior. If the temperature reading increases by more than 2°C this is recorded as a freezing event (Figure 2c). The 2°C threshold occasionally needs to be

optimised to capture freezing events while eliminating false positive detection of freezing. For example, samples that freeze within ~3°C of melting are more difficult to detect since the maximum temperature of an aliquot of water-ice is 0°C and the threshold has to be reduced to below 2°C; manual inspection is required in this temperature regime. The code then prints out the number of events recorded, along with a time vs temperature plot (Figure 2b) and the corresponding event temperatures for the user to quality control check and then exports the data as a '.csv' file.

The whole process from sample preparation to final analysis takes approximately 1 hour. In order to achieve higher throughput of samples, albeit with a reduced number of replicates, multiple samples and internal blanks can be placed within one multiwell plate. For example, when performing dilutions we might run 12 wells as a handling blank and three lots of 28 wells that contain three different sample dilutions. This not only speeds up analysis, it also reduces run-to-run variability and the aging of a sample in water.

2.3 Temperature measurements with an Infrared camera

By using an IR camera to view the thermal emission of each individual well of suspension we are able to obtain temperatures associated with individual wells. This contrasts with the approaches adopted in other experiments where the temperature is recorded, for example when employing a cold stage housing an embedded thermocouple whose reading is assumed to be representative for all droplets. We note that in our system there was a lateral gradient across the entire multiwell plate in the IR-NIPI of up to 6°C (in extreme cases). This is likely due to there not being an even thermal contact of the multiwell plate with the underlying cold plate. The typical gradient was 4°C, hence temperature measurements of the individual wells was necessary.

2.4 Temperature calibration

Our calibration is based on the fact that when an aliquot of water in a multiwell plate freezes, the released latent heat raises the temperature of the aliquot to the ice-water equilibrium temperature (0°C when the water activity of the sample is ~1, as it is in these experiments). This is illustrated in Figure 2c which shows the phases of crystallisation that the aliquots go through. Initially, the crystal growth is rapid with a rapid release of latent heat and a corresponding rise in temperature of the aliquot within the 20 s time between frames. Visual inspection of the IR camera output revealed that the temperature reached a maximum within 1 s. The temperature of an ice-water mixture will necessarily be 0°C, hence the aliquot cannot warm above 0°C and the temperature will remain

at 0°C until all of the water has frozen and no more heat is evolved. The rate of crystallisation in this regime is determined by the loss of heat to the surroundings, in this case the cold stage, as well as to the surrounding droplets and the multiwell plate. This stage of crystallisation takes longer at higher freezing temperatures where the temperature differential between the cold stage and the aliquot is smaller. Hence, freezing when nucleation takes place at -12°C takes around 100 s, whereas when nucleation takes place at -20°C freezing takes around 20-40 s. Once all of the water has frozen the temperature of the aliquot decreases rapidly back to that of the multiwell plate within 20-40 s. The fact that the aliquots spend 10s of seconds at 0°C provides a very useful calibration point for each individual well. In the following we describe a novel method for calibrating the IR temperature measurements that takes advantage of this process and proceed to justify this approach.

Using the analysis code, when an event is identified it uses the recorded temperature of the frame after the initial event and calculates the difference of this value compared to 0°C to give an offset correction value. This offset value is then subtracted from the temperature recordings for that specific well. The average correction value calculated for the IR camera via this method is -1.9°C with a standard deviation 0.5°C.

We performed a number of experiments to test the IR temperature measurement calibrated using the above method. In the first instance we used highly conductive individual aluminium wells for 50µL droplets. The temperature of these wells were recorded independently using T type thermocouples embedded in the aluminium wells to give a representative temperature of the well and aliquot of water (see inset in Figure 3). A standard freezing experiment was then performed and the thermocouple data was contrasted to that of the IR camera which was calibrated using the above method (Figure 3). The comparison in Fig 3a shows that the IR and thermocouple temperature were in excellent agreement and this is also readily seen in residuals plotted in Fig 3b. The scatter around the zero line in the residual plot is ± 0.9°C (two standard deviations) in the regime after the equilibration at 5°C and before the first freezing event. We used this value as an estimate of the temperature uncertainty associated with the IR technique generally.

We also tested the IR temperature measurement using T type thermocouples distributed in specific wells of a polypropylene multiwell plate. The IR camera could not take an accurate reading of wells that had a thermocouple placed inside them, therefore neighbouring unfrozen wells were assumed to be representative of each other (see inset in Figure 4). As mentioned above there is a gradient across the entire plate and so a series of preliminary experiments were undertaken to find suitable placement locations for the thermocouples in which the surrounding wells displayed similar temperature readings compared to one another. The thermocouples were placed in the base

of the well along with 50 µL of Milli-Q grade water and four surrounding well temperatures were measured using the IR system. The thermocouple wire crossed one of the four IR measured wells and so only three wells adjacent to the thermocouple monitored well were used for comparison.

A total of six IR measurements were recorded with the corresponding thermocouple readings over a series of experiments spanning a temperature range of 20°C to –25°C. An example of a thermocouple measurement contrasted to three IR measurements can be seen in Figure 4a.The residual temperatures for all six thermocouple temperatures are also shown (Figure 4b). The IR temperature uncertainty derived from the aluminium well experiment is also plotted and shows that the data is consistent across both strategies with an uncertainty of ± 0.9°C.

3 Test experiments and analysis

3.1 Control experiments

In larger volume freezing assays (10s of microliters) it is extremely challenging to remove all background INPs from the water and substrates, hence freezing is typically observed at temperatures well above what one would expect for homogenous freezing (Koop and Murray, 2016). Homogeneous nucleation is expected to result in 50% of 50 µl droplets freezing at around -35°C see, whereas 50% of the Milli-Q water droplets froze around -22°C in our control experiments (Figure 5). Filtering of the Milli-Q water to 0.22 µm reduced the temperature at which pure water droplets froze. Blanks were run initially with entire 96 well plates and then 12 wells of each experiment thereafter were allocated for an internal blank when testing samples of INPs (i.e. 12 aliquots of Milli-Q water and 84 aliquots of sample suspension). Comparison of fraction frozen curves for typical IR-NIPI blanks with curves obtained for droplets containing various ice-nucleating materials (discussed below) show that there is a clear heterogeneous freezing signal (Figure 5). We hope to improve the baseline in the future (Polen et al., 2018) but for the purpose of these experiments the nucleants tested were active at sufficiently warm temperatures to be well above the baseline.

3.3 Feldspar chips

To further test the temperature readings from the IR-NIPI instrument a set of experiments was performed where each droplet contained a single ~100 µm sized grain of K-feldspar, a mineral known to exhibit excellent ice-nucleating properties (Atkinson et al., 2013; Harrison et al., 2016). This experiment was adapted from the

procedure described by Whale *et al*. (2018) and involved taking feldspar chips from a bulk rock of pegmatite and selecting individual grains. Pegmatite is an igneous intrusive rock rich in felsic minerals (including alkali feldspars) with grain sizes often being larger than 2.5cm. The feldspar chips were selected after sorting them by eye. A total of 20 grains were collected, assigned a number and their position tracked through the course of each experiment. The same feldspar chips were tested in both the µL-NIPI and the IR-NIPI. For the IR-NIPI experiments single grains of feldspar were placed into the bottom of a multiwell plate and 50 µL of Milli-Q water was then pipetted into each well. The experiment was then carried out as normal and the freezing temperatures of the wells were recorded. The grains were then used in the µL-NIPI experiment by placing the grains onto a glass cover slip atop a cold plate and pipetting 1 µL droplets onto the grains, before carrying out a standard µL-NIPI experiment as described by Whale *et al.* (2015). Briefly, the temperature of the cold plate was reduced at 1°C min^{-1} and the temperature of the droplet freezing events recorded via a camera. The resulting fraction frozen plot for this experiment can be seen in Figure 6. The two instruments yielded similar fraction frozen curves, with the agreement between the two suggesting that the temperature measurement and calibration of the IR-NIPI were robust. The agreement also further justified the use of the calibration method developed for the IR camera. The observation that the feldspar grains in the two experiments gave rise to similar results suggests that the IR camera is reporting a representative temperature, within the quoted temperature uncertainties.

3.4 NX-illite

The mineral dust NX-illite was chosen as a test sample as it has been used in an extensive intercomparison study (Hiranuma et al. 2015) and contains some common components which are found in atmospheric mineral dusts (Broadley et al., 2012). NX-illite was taken from the same batch as that used by the Leeds group in the Hiranuma *et al.* (2015) intercomparison and no further processing of the material was carried out. Aqueous suspensions of the sample were prepared by weighing a known amount of material and suspending it in a corresponding volume of water to make up a weight percent suspension (i.e. 0.1 g of mineral in 9.9 g of water to yield a 1 wt% suspension). NX-illite concentrations of 0.01, 0.1 and 1 wt% were prepared in this manner, and in each case a Teflon-coated magnetic stirrer bar was used to keep the particles suspended whilst the sample was pipetted into the wells of the multiwell plate. Each concentration of NX-illite was tested using the IR-NIPI and the resultant fraction frozen curves are shown in Fig. 5.

Atmos. Meas. Tech. Discuss., https://doi.org/10.5194/amt-2018-177
Manuscript under review for journal Atmos. Meas. Tech.
Discussion started: 13 June 2018

Atmospheric Measurement Techniques Discussions

By employing a suspension of known concentration and composed of a material with a known specific surface area, the surface area of nucleator per droplet can be calculated and used alongside the fraction frozen curves to determine $n_s(T)$, as described in equation (1). The $n_s(T)$ values derived from the IR-NIPI for 0.01, 0.1 and 1 wt% NX-illite are shown in Figure 7a. The results demonstrated good agreement with each other and exhibited the expected trend of the lower wt% droplets freezing at lower temperatures and having higher $n_s(T)$ values than the droplets having higher wt% suspensions. Further to this, a freeze-thaw experiment of a 0.1 wt% NX-illite suspension was conducted wherein the sample was frozen once, thawed and then frozen again (see Figure 8). The two runs froze at similar temperatures, as expected, showing good reproducibility with the IR-NIPI technique.

The n_s derived from IR-NIPI with 0.01, 0.1 and 1 wt% NX-illite are shown in Figure 7a. They are in good agreement with one another with lower wt% suspensions yielding data at lower temperatures and higher n_s values, as expected. Further to this a freeze thaw experiment of 0.1wt% suspension was conducted where the sample was frozen once, thawed and then frozen again (see Figure 8). The agreement between the two runs show that the material did not alter on freezing.

The values of $n_s(T)$ for NX-illite derived from 0.01-1 wt% suspensions are shown in Figure 7a, and is illustrated together with the literature data for this material in Figure 7b. This material has also been investigated by Beall *et al*. (2017) using an instrument that also takes advantage of 50µL droplets: the Automated Ice Spectrometer (AIS). The results of Beall *et al*. (2017) are therefore directly comparable to the results from the IR-NIPI. All of the wet suspension techniques have been grouped together in black in Fig. 7b, apart from the AIS data shown in green and the IR-NIPI data in red. Both the IR-NIPI and AIS data were in good agreement with one another. It can be seen that the larger volume assays (IR-NIPI and AIS) gave results towards the upper spread of literature data but are still consistent with other results (Figure 7b). Dry dispersed techniques have also been plotted as unfilled blue squares in Fig. 7b, but none of these techniques were sensitive in the range of $n_s(T)$ seen by the large droplet instruments. The new data from the IR-NIPI has extended the dataset for NX-illite to warmer temperatures than in previous measurements, illustrating the utility of the technique.

It should be noted that in preliminary experiments some discrepancies between dilutions of NX-illite were observed which highlighted the importance of accurately making up suspensions. In the flowing we note some issues that had to be solved. In some initial experiments the dilutions of a suspension would yield a higher than expected $n_s(T)$. On further investigation this issue was resolved via gravimetrically weighing suspensions (i.e.

preparing a known mass of a sample in a known mass of water) rather than diluting a bulk stock suspension. Further to this great care was taken when sampling from the bulk NX-illite sample as to make sure no bias was introduced when selecting material since a powder can separate on the basis of grain size. This was avoided by shaking the container horizontally and selecting material from the centre of the bulk sample. Magnetic stirrer bars were used to keep particles suspend but when it came to collecting the suspension using a pipette the suspension was taken from the magnetic stirrer plate to stop the vortex within the vial. As the suspension was not stirring for a short period of time it meant that particles did not have time to fallout of suspension and there was no longer a vortex created by the stirrer bar which could bias particle distribution when sampling. The above emphasises the importance of selecting samples in a repeatable way and may explain some of the variability between the literature data seen in Fig. 7b.

3.4 Atmospheric aerosol sample

In order to demonstrate the utility of this approach for atmospheric aerosol samples, filter samples were collected in Leeds as part of a field campaign held on the evening of the 5th November. Samples of atmospheric aerosol were collected using a Mesa PQ100 air sampler for 100 min. An inlet head with an upper cut-off of 10µm was utilised and air was sampled at 16.7 L min^{-1} on to 0.4 µm polycarbonate track-etched Whatman filters, with a total of 167 L of air sampled. The filters were then placed in to 6 mL of Milli-Q water and vortexed for 5 min to wash the particles from the filter and into suspension.

The aqueous sample was then analysed on the IR-NIPI and µL-NIPI (Whale et al., 2015). The concentration of INPs per litre of air, $[INP]_T$, was subsequently calculated using equation (2) (DeMott et al., 2016).

$$[INP]_T = -\ln\left(\frac{Nu(T)}{N}\right)\left(\frac{V_w}{V_a V_s}\right) \quad (2)$$

Where N_U(T) is the number of unfrozen droplets at a given temperature, N is the total number of droplets, V_w is the volume of wash water, V_a is the volume of an aliquot and V_s is the volume of air sampled.

The resulting INP concentrations from the combination of these two instruments spanned four orders of magnitude and covered a temperature range of 20°C (see Figure 9). The data from both instruments was in good agreement and yielded complementary information. This illustrates how the IR-NIPI can be used to extend the measurements of INP concentrations to higher temperatures and lower INP concentrations. Since modelling suggests that 0.1 to 1 INP L^{-1} is a critical concentration and much lower concentrations still impact clouds (Vergara-Temprado et al.,

2018), measurements with IR-NIPI will be extremely useful, particularly in environments with low INP concentrations.

4 Summary and conclusions

The IR-NIPI technique is a novel approach to measuring freezing events in immersion mode nucleation studies. We demonstrate that IR thermometry is a sound method for determining the freezing temperature of 50 µL water droplets in multiwell plates, overcoming potential distorting influences such as gradients, neighbouring wells freezing and poor thermal contact. A novel calibration method has been proposed which relies on the return of water droplets to the equilibrium melting temperature of water, 0°C, after initial freezing. This gives an individual calibration for every run and every well. When comparing this calibration technique to thermocouple readings the data is consistent to within ±0.9°C. The use of this calibration method is further supported when looking at experiments using single grains of feldspar, with the results being consistent with those of the established µL-NIPI instrument that employs 1µL droplets on a cold stage. Results for the ice nucleating ability of NX-illite with the IR-NIPI, a mineral dust which has been the subject of an extensive inter-comparison, are consistent with literature measurements. In particular, the IR-NIPI is in good agreement with another well-characterised large droplet instrument (AIS) (Beall et al., 2017). However, it is unclear why both of these large volume instruments produce n_s results at the high end of the range of n_s values reported previously. The utility of IR-NIPI for the analysis of atmospheric samples was also demonstrated by collecting and analysing an aerosol sample in the atmosphere of the city of Leeds, England. The sample was analysed simultaneously with the µL-NIPI instrument. Results from the two instruments were in good agreement with one another. The IR-NIPI instrument extended the range of INP concentrations shown by the µL-NIPI by two orders of magnitude, covering a regime critical for cloud formation with a modest sampling time of just 100 mins at 16.67 L min^{-1}. The use of the multiwell plates and the IR camera lends the IR-NIPI to the possibility of automating the system further and this is an objective for future work.

5 REFERENCES

Atkinson, J.D., Murray, B.J., Woodhouse, M.T., Whale, T.F., Baustian, K.J., Carslaw, K.S., Dobbie, S., O'Sullivan, D. and Malkin, T.L. 2013. The importance of feldspar for ice nucleation by mineral dust in mixed-phase clouds. *Nature.* **498**(7454), pp.355-358.

Beall, C.M., Stokes, M.D., Hill, T.C., DeMott, P.J., DeWald, J.T., DeWald, J.T. and Prather, K.A. 2017. Automation and heat transfer characterization of immersion mode spectroscopy for analysis of ice nucleating particles. *Atmospheric Measurement Techniques.* **10**(7), pp.2613-2626.

Bigg, E.K. 1953. The supercooling of water. *Proc.Phys. Soc.* **66**, pp.688-694.

343 Broadley, S.L., Murray, B.J., Herbert, R.J., Atkinson, J.D., Dobbie, S., Malkin, T.L., Condliffe, E. and
344 Neve, L. 2012. Immersion mode heterogeneous ice nucleation by an illite rich powder
345 representative of atmospheric mineral dust. *Atmos. Chem. Phys.* **12**(1), pp.287-307.
346 Budke, C. and Koop, T. 2015. BINARY: an optical freezing array for assessing temperature and time
347 dependence of heterogeneous ice nucleation. *Atmos. Meas. Tech.* **8**(2), pp.689-703.
348 Conen, F., Morris, C.E., Leifeld, J., Yakutin, M.V. and Alewell, C. 2011. Biological residues define the
349 ice nucleation properties of soil dust. *Atmos. Chem. Phys.* **11**(18), pp.9643-9648.
350 Connolly, P.J., Möhler, O., Field, P.R., Saathoff, H., Burgess, R., Choularton, T. and Gallagher, M.
351 2009. Studies of heterogeneous freezing by three different desert dust samples. *Atmos.*
352 *Chem. Phys.* **9**(8), pp.2805-2824.
353 Cotton, R.J., Benz, S., Field, P.R., Mohler, O. and Schnaiter, M. 2007. Technical note: A numerical
354 test-bed for detailed ice nucleation studies in the AIDA cloud simulation chamber. *Atmos.*
355 *Chem. Phys.* **7**, pp.243-256.
356 DeMott, P.J. 1995. Quantitative Descriptions of Ice Formation Mechanisms of Silver Iodide-Type
357 Aerosols. *Atmospheric Research.* **38**(1-4), pp.63-99.
358 DeMott, P.J., Hill, T.C., McCluskey, C.S., Prather, K.A., Collins, D.B., Sullivan, R.C., Ruppel, M.J.,
359 Mason, R.H., Irish, V.E., Lee, T., Hwang, C.Y., Rhee, T.S., Snider, J.R., McMeeking, G.R.,
360 Dhaniyala, S., Lewis, E.R., Wentzell, J.J., Abbatt, J., Lee, C., Sultana, C.M., Ault, A.P., Axson,
361 J.L., Diaz Martinez, M., Venero, I., Santos-Figueroa, G., Stokes, M.D., Deane, G.B., Mayol-
362 Bracero, O.L., Grassian, V.H., Bertram, T.H., Bertram, A.K., Moffett, B.F. and Franc, G.D. 2016.
363 Sea spray aerosol as a unique source of ice nucleating particles. *Proc Natl Acad Sci U S A.*
364 **113**(21), pp.5797-5803.
365 Diehl, K. and Mitra, S.K. 1998. A laboratory study of the effects of a kerosene-burner exhaust on ice
366 nucleation and the evaporation rate of ice crystals. *Atmospheric Environment.* **32**(18),
367 pp.3145-3151.
368 Du, R., Du, P., Lu, Z., Ren, W., Liang, Z., Qin, S., Li, Z., Wang, Y. and Fu, P. 2017. Evidence for a missing
369 source of efficient ice nuclei. *Sci Rep.* **7**, p39673.
370 Eidhammer, T., DeMott, P.J., Prenni, A.J., Petters, M.D., Twohy, C.H., Rogers, D.C., Stith, J.,
371 Heymsfield, A., Wang, Z., Pratt, K.A., Prather, K.A., Murphy, S.M., Seinfeld, J.H.,
372 Subramanian, R. and Kreidenweis, S.M. 2010. Ice Initiation by Aerosol Particles: Measured
373 and Predicted Ice Nuclei Concentrations versus Measured Ice Crystal Concentrations in an
374 Orographic Wave Cloud. *Journal of the Atmospheric Sciences.* **67**(8), pp.2417-2436.
375 Garcia, E., Hill, T.C.J., Prenni, A.J., DeMott, P.J., Franc, G.D. and Kreidenweis, S.M. 2012. Biogenic ice
376 nuclei in boundary layer air over two U.S. High Plains agricultural regions. *Journal of*
377 *Geophysical Research-Atmospheres.* **117**.
378 Harrison, A.D., Whale, T.F., Carpenter, M.A., Holden, M.A., Neve, L., apos, Sullivan, D., Vergara
379 Temprado, J. and Murray, B.J. 2016. Not all feldspars are equal: a survey of ice nucleating
380 properties across the feldspar group of minerals. *Atmospheric Chemistry and Physics.* **16**(17),
381 pp.10927-10940.
382 Herbert, R.J., Murray, B.J., Dobbie, S.J. and Koop, T. 2015. Sensitivity of liquid clouds to homogenous
383 freezing parameterizations. *Geophysical Research Letters.* **42**(5), pp.1599-1605.
384 Herbert, R.J., Murray, B.J., Whale, T.F., Dobbie, S.J. and Atkinson, J.D. 2014. Representing time-
385 dependent freezing behaviour in immersion mode ice nucleation. *Atmospheric Chemistry*
386 *and Physics.* **14**(16), pp.8501-8520.
387 Hiranuma, N., Augustin-Bauditz, S., Bingemer, H., Budke, C., Curtius, J., Danielczok, A., Diehl, K.,
388 Dreischmeier, K., Ebert, M., Frank, F., Hoffmann, N., Kandler, K., Kiselev, A., Koop, T., Leisner,
389 T., Möhler, O., Nillius, B., Peckhaus, A., Rose, D., Weinbruch, S., Wex, H., Boose, Y., DeMott,
390 P.J., Hader, J.D., Hill, T.C.J., Kanji, Z.A., Kulkarni, G., Levin, E.J.T., McCluskey, C.S., Murakami,
391 M., Murray, B.J., Niedermeier, D., Petters, M.D., O'Sullivan, D., Saito, A., Schill, G.P., Tajiri, T.,
392 Tolbert, M.A., Welti, A., Whale, T.F., Wright, T.P. and Yamashita, K. 2015. A comprehensive

laboratory study on the immersion freezing behavior of illite NX particles: a comparison of 17 ice nucleation measurement techniques. *Atmos. Chem. Phys.* **15**(5), pp.2489-2518.

Hoose, C., Kristjánsson, J.E., Chen, J.-P. and Hazra, A. 2010. A Classical-Theory-Based Parameterization of Heterogeneous Ice Nucleation by Mineral Dust, Soot, and Biological Particles in a Global Climate Model. *Journal of the Atmospheric Sciences.* **67**(8), pp.2483-2503.

Hoose, C. and Möhler, O. 2012. Heterogeneous ice nucleation on atmospheric aerosols: a review of results from laboratory experiments. *Atmos. Chem. Phys.* **12**(20), pp.9817-9854.

Kanji, Z.A., Ladino, L.A., Wex, H., Boose, Y., Burkert-Kohn, M., Cziczo, D.J. and Krämer, M. 2017. Overview of Ice Nucleating Particles. *Meteorological Monographs.* **58**, pp.1.1-1.33.

Knopf, D.A. and Alpert, P.A. 2013. A water activity based model of heterogeneous ice nucleation kinetics for freezing of water and aqueous solution droplets. *Faraday Discuss.* **165**(0), pp.513-534.

Knopf, D.A. and Forrester, S.M. 2011. Freezing of Water and Aqueous NaCl Droplets Coated by Organic Monolayers as a Function of Surfactant Properties and Water Activity. *J. Phys. Chem. A.* **115**(22), pp.5579-5591.

Koop, T. and Murray, B.J. 2016. A physically constrained classical description of the homogeneous nucleation of ice in water. *J Chem Phys.* **145**(21), p211915.

Murray, B.J., Broadley, S.L., Wilson, T.W., Atkinson, J.D. and Wills, R.H. 2011. Heterogeneous freezing of water droplets containing kaolinite particles. *Atmos. Chem. Phys.* **11**(9), pp.4191-4207.

Murray, B.J., O'Sullivan, D., Atkinson, J.D. and Webb, M.E. 2012. Ice nucleation by particles immersed in supercooled cloud droplets. *Chemical Society Reviews.* **41**, pp.6519-6554.

Niemand, M., Möhler, O., Vogel, B., Vogel, H., Hoose, C., Connolly, P., Klein, H., Bingemer, H., DeMott, P., Skrotzki, J. and Leisner, T. 2012. A Particle-Surface-Area-Based Parameterization of Immersion Freezing on Desert Dust Particles. *Journal of the Atmospheric Sciences.* **69**(10), pp.3077-3092.

Pitter, R.L. and Pruppacher, H.R. 1973. Wind-tunnel investigation of freezing of small water drops falling at terminal velocity in air. *Quarterly Journal of the Royal Meteorological Society.* **99**(421), pp.540-550.

Rogers, D.C., DeMott, P.J., Kreidenweis, S.M. and Chen, Y.L. 2001. A continuous-flow diffusion chamber for airborne measurements of ice nuclei. *J. Atmos. Ocean. Tech.* **18**(5), pp.725-741.

Salam, A., Lohmann, U., Crenna, B., Lesins, G., Klages, P., Rogers, D., Irani, R., MacGillivray, A. and Coffin, M. 2006. Ice nucleation studies of mineral dust particles with a new continuous flow diffusion chamber. *Aerosol. Sci. Tech.* **40**(2), pp.134-143.

Sear, R.P. 2014. Quantitative studies of crystal nucleation at constant supersaturation: experimental data and models. *CrystEngComm.* **16**(29), pp.6506-6522.

Stopelli, E., Conen, F., Zimmermann, L., Alewell, C. and Morris, C.E. 2014. Freezing nucleation apparatus puts new slant on study of biological ice nucleators in precipitation. *Atmospheric Measurement Techniques.* **7**(1), pp.129-134.

Storelvmo, T., Hoose, C. and Eriksson, P. 2011. Global modeling of mixed-phase clouds: The albedo and lifetime effects of aerosols. *Journal of Geophysical Research: Atmospheres.* **116**(D5), pD05207.

Vali, G. 1971. Quantitative Evaluation of Experimental Results an the Heterogeneous Freezing Nucleation of Supercooled Liquids. *Journal of the Atmospheric Sciences.* **28**(3), pp.402-409.

Vali, G. 1994. Freezing Rate Due to Heterogeneous Nucleation. *Journal of the Atmospheric Sciences.* **51**(13), pp.1843-1856.

Vali, G. 1995. Principles of Ice Nucleation. In: Lee Jr, R., Warren, G. J., and Gusta, L. V. ed. *Biological Ice Nucleation and Its Applications.* St. Paul, Mn, USA: American Phytopathological Society, pp.1-28.

Vali, G. 2008. Repeatability and randomness in heterogeneous freezing nucleation. *Atmos. Chem. Phys.* **8**(16), pp.5017-5031.

444 Vali, G., DeMott, P.J., Möhler, O. and Whale, T.F. 2015. Technical Note: A proposal for ice nucleation
445 terminology. *Atmos. Chem. Phys.* **15**(18), pp.10263-10270.
446 Vergara-Temprado, J., Miltenberger, A.K., Furtado, K., Grosvenor, D.P., Shipway, B.J., Hill, A.A.,
447 Wilkinson, J.M., Field, P.R., Murray, B.J. and Carslaw, K.S. 2018. Strong control of Southern
448 Ocean cloud reflectivity by ice-nucleating particles. *Proc Natl Acad Sci U S A.* **115**(11),
449 pp.2687-2692.
450 Vergara-Temprado, J., Murray, B.J., Wilson, T.W., amp, apos, Sullivan, D., Browse, J., Pringle, K.J.,
451 Ardon-Dryer, K., Bertram, A.K., Burrows, S.M., Ceburnis, D., DeMott, P.J., Mason, R.H., amp,
452 apos, Dowd, C.D., Rinaldi, M. and Carslaw, K.S. 2017. Contribution of feldspar and marine
453 organic aerosols to global ice nucleating particle concentrations. *Atmospheric Chemistry and*
454 *Physics.* **17**(5), pp.3637-3658.
455 Whale, T.F., Murray, B.J., O'Sullivan, D., Wilson, T.W., Umo, N.S., Baustian, K.J., Atkinson, J.D.,
456 Workneh, D.A. and Morris, G.J. 2015. A technique for quantifying heterogeneous ice
457 nucleation in microlitre supercooled water droplets. *Atmos. Meas. Tech.* **8**(6), pp.2437-2447.

458

459

460

461

462

463

464

465

466

467

468

469

Atmos. Meas. Tech. Discuss., https://doi.org/10.5194/amt-2018-177
Manuscript under review for journal Atmos. Meas. Tech.
Discussion started: 13 June 2018

Atmospheric Measurement Techniques Discussions

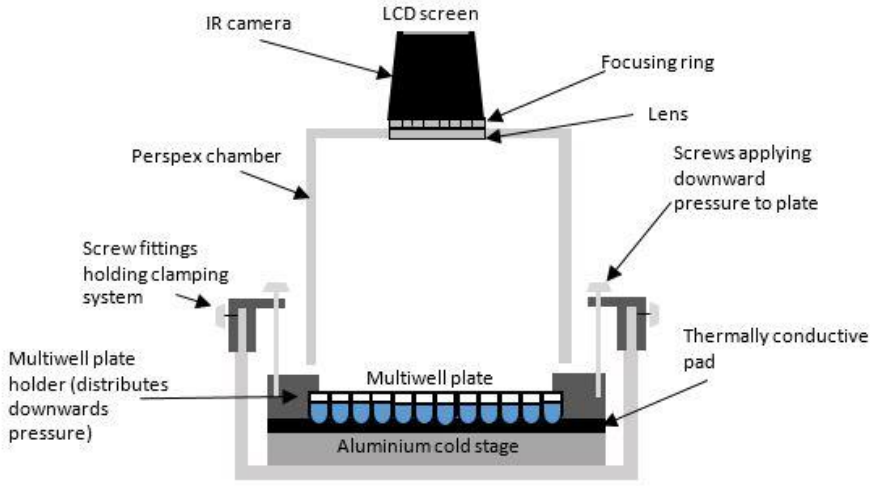

470

471 **Figure 1**. Schematic diagram of the IR-NIPI system (not to scale). The IR camera is positioned above the multiwell plate and monitors the
472 freezing events as the cold stage cools.

473

474

475

Atmos. Meas. Tech. Discuss., https://doi.org/10.5194/amt-2018-177
Manuscript under review for journal Atmos. Meas. Tech.
Discussion started: 13 June 2018

Atmospheric Measurement Techniques Discussions

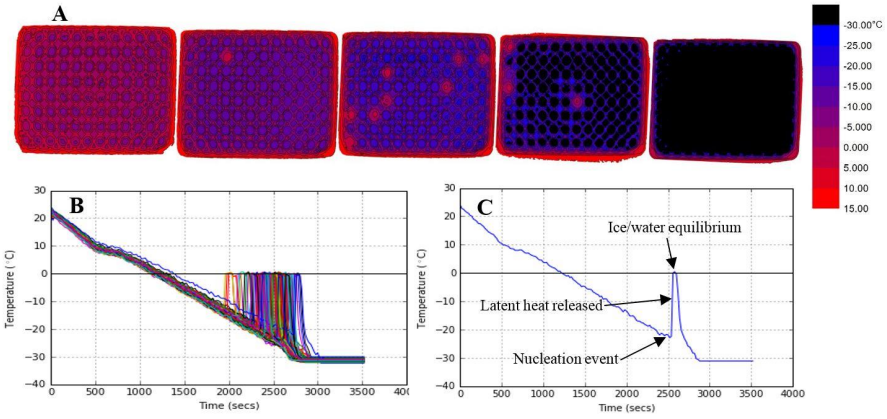

Figure 2. (a) Demonstrates a sequence of colour maps taken during the course of an experiment. The leftmost image shows the start of an experiment with all droplets unfrozen, moving to all droplets frozen in the right most image**.** Warmer temperatures are represented in red, transitioning to blue for colder temperatures and finally black at -30°C and below. **(b)** An example of the output of each experiment with the temperature of the 96 wells plotted against time. The spikes in temperature are related to ice formation. The gradient of the decreasing temperature is consistent with that of 1°C min^{-1}. The calibration described in section 2.2 was applied here. **(c)** Plot of temperature vs time for a single well within a multiwell plate containing 50µLs of water.

Atmos. Meas. Tech. Discuss., https://doi.org/10.5194/amt-2018-177
Manuscript under review for journal Atmos. Meas. Tech.
Discussion started: 13 June 2018

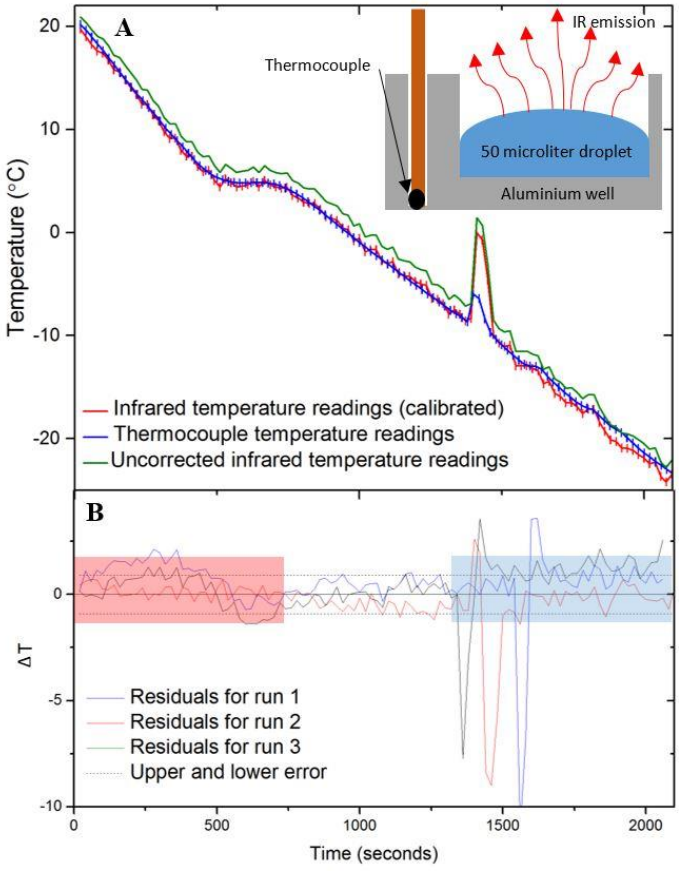

Figure 3. (a) Plot showing a temperature measurement from a thermocouple (shown in blue) placed within an aluminium well vs infrared measurements taken using the IR camera. Uncorrected IR data is shown in green, whilst corrected IR data following the calibration described in section 2.2 is shown in red. Inset is a schematic of the experimental setup. **(b)** Plot illustrating the difference in temperature between the thermocouple readings for three aluminium wells and the corresponding IR data. The calculated error in temperature for the IR camera of ± 0.9°C is shown in dashed lines. The point of freezing is highlighted in blue as this is where the thermal properties of ice and the initiation of heat release will affect the temperature readings. Highlighted in red is the section of data before the well has equilibrated and so the IR camera is likely reading a warmer surface temperature than the thermocouple.

Atmos. Meas. Tech. Discuss., https://doi.org/10.5194/amt-2018-177
Manuscript under review for journal Atmos. Meas. Tech.
Discussion started: 13 June 2018

Atmospheric Measurement Techniques Discussions

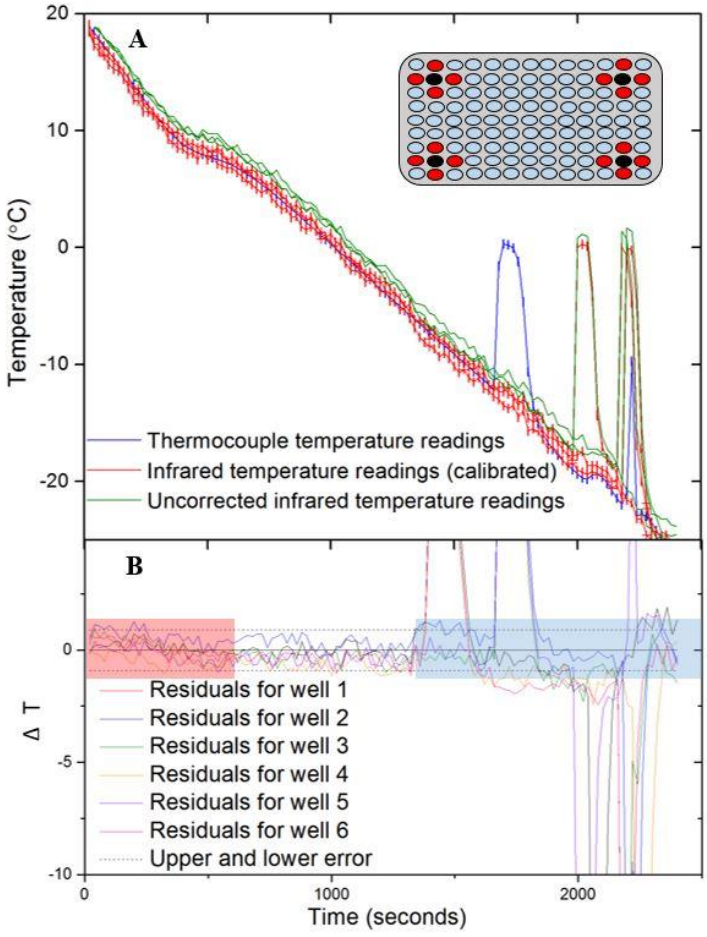

Figure 4. (a) Plot showing a temperature measurement from a thermocouple placed within a polyethylene well vs three infrared measurements of surrounding wells corrected using the calibration described in section 2.2. The uncorrected IR data can be seen in green, with the corrected IR data in red and the thermocouple readings in blue. A schematic diagram of the experiment is shown of the wells within a 96 well plate chosen for temperature checks. Red wells represent the wells measured with the infrared camera and black wells represent those measured with thermocouples. It should be noted that one of the four surrounding IR well temperature readings was discarded from each experiment as the thermocouple wire impeded the temperature measurement **(b)** Plot of the difference in temperature between the thermocouple readings for two wells and six corresponding wells measured with the IR camera. The calculated error in temperature for the IR camera is shown in dashed lines (±0.9°C). The range of freezing is highlighted in blue as this is where the thermal properties of ice and the initiation of heat release will affect the temperature readings. Highlighted in red is the section of data before the well had equilibrated and so the IR camera was likely reading a warmer surface temperature than the thermocouple.

Atmos. Meas. Tech. Discuss., https://doi.org/10.5194/amt-2018-177
Manuscript under review for journal Atmos. Meas. Tech.
Discussion started: 13 June 2018

Atmospheric Measurement Techniques Discussions

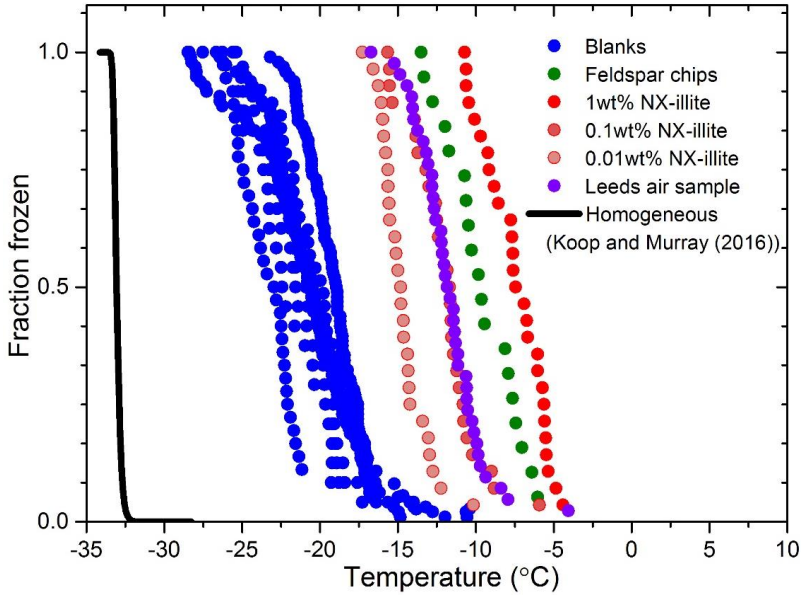

Figure 5. Plot of the fraction frozen curves for the IR-NIPI experiment showing blanks and sample runs. Homogeneous freezing of water as predicted with the Koop and Murray (2016) parameterisation is also shown in black.

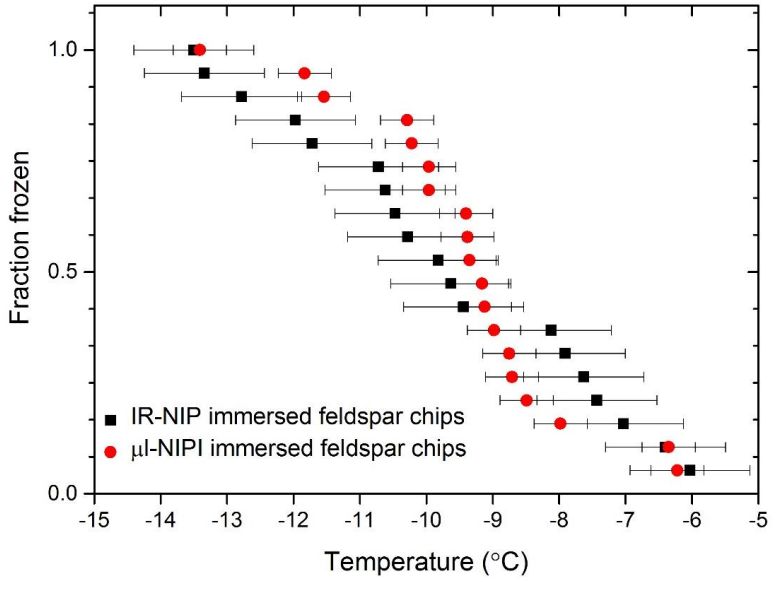

Atmos. Meas. Tech. Discuss., https://doi.org/10.5194/amt-2018-177
Manuscript under review for journal Atmos. Meas. Tech.
Discussion started: 13 June 2018

Atmospheric Measurement Techniques Discussions

Figure 6. Plot of the fraction frozen curves for single feldspar particles per droplet in both the µL-NIPI (using 1 µL droplets) and IR-NIPI (using 50 µL droplets) experiments.

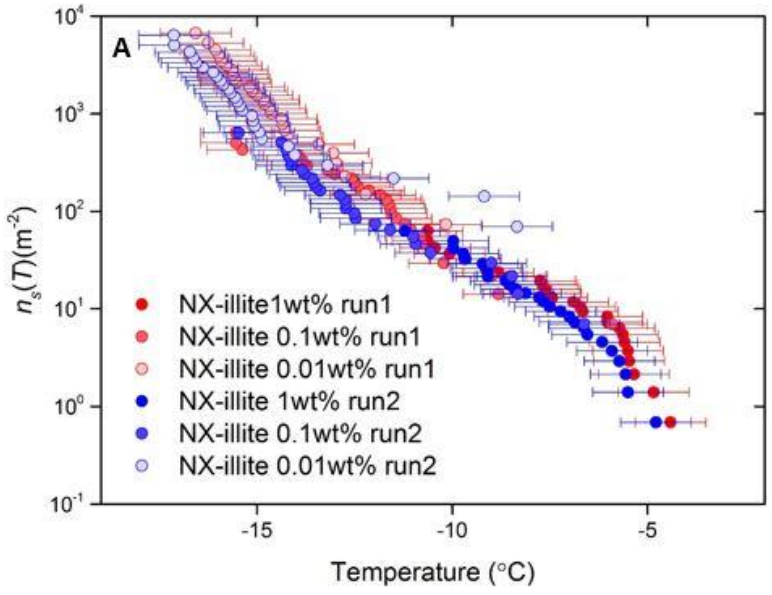

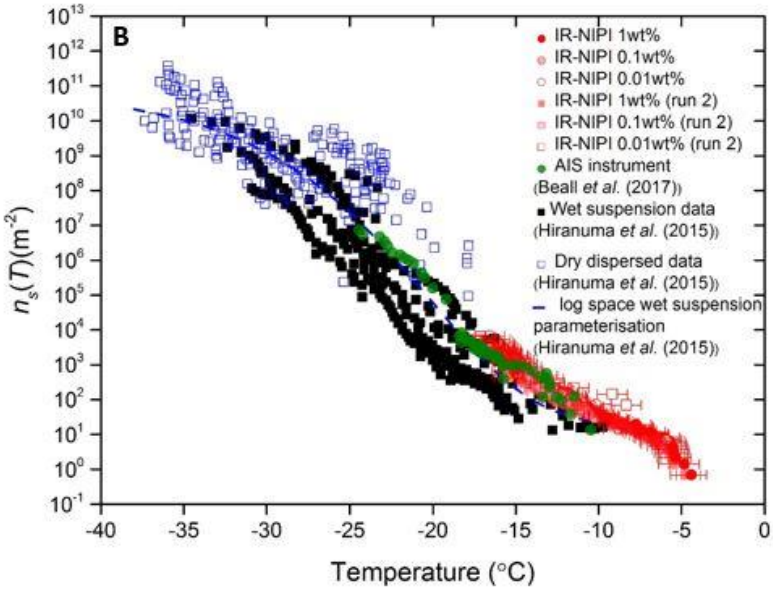

Figure 7. (a) The active site density, $n_s(T)$, for a dilution series of NX-illite run on the IR-NIPI instrument. The data for a repeat experiment is also shown **(b)** Plot of the active site density vs temperature for an array of techniques investigating NX-illite. Data from wet dispersed techniques are displayed in black with the IR-NIPI highlighted in red and Automated Ice Spectrometer (AIS) in green. Data from dry dispersed techniques are also plotted as hollow blue squares.

Atmos. Meas. Tech. Discuss., https://doi.org/10.5194/amt-2018-177
Manuscript under review for journal Atmos. Meas. Tech.
Discussion started: 13 June 2018

Atmospheric Measurement Techniques Discussions

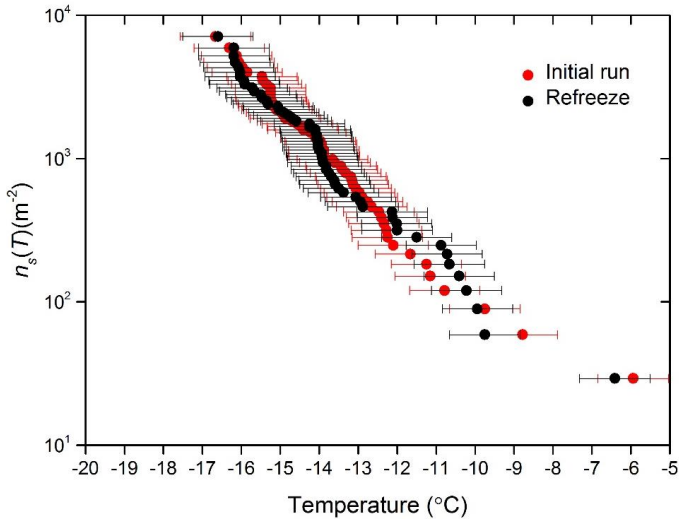

Figure 8. Plot of the active site density, $n_s(T)$, for a 0.01wt% NX-illite suspension and its corresponding refreeze run after the droplets had been thawed out.

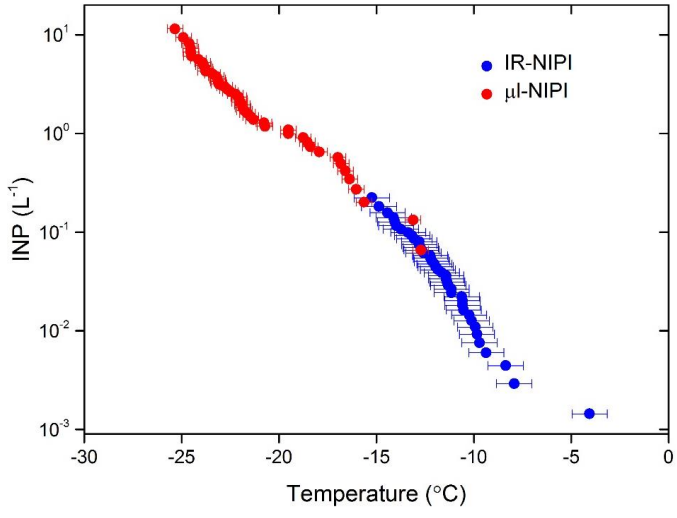

Figure 9. INP concentrations per litre of sampled air during a field campaign. INP concentrations are displayed for the IR-NIPI and µL-NIPI.